Cognitive Neurodynamics (2025) 19:173
https://doi.org/10.1007/s11571-025-10354-7

RESEARCH ARTICLE

Dynamic brain connectivity: linking inter-group difference and individual susceptibility changes in visually induced motion sickness susceptibility

Yixuan Wang[1,2] · Yue Wei[1,2] · Richard H. Y. So[3,4] · Yuka O. Okazaki[5,6] · Keiichi Kitajo[5,6]

Received: 13 November 2024 / Revised: 12 August 2025 / Accepted: 23 September 2025 / Published online: 4 November 2025

Abstract

Visually induced motion sickness (VIMS) is a prevalent discomfort experienced in virtual environments, and individual susceptibility to VIMS can change with training or experience. Currently, the neurological activities that respond to susceptibility changes remain unclear. This study identified dynamic brain connectivity that consistently responded to inter-group susceptibility differences as well as individual susceptibility changes. Participants with varying susceptibility to VIMS underwent adaptation training, which involved repeated exposure to roll rotation stimulation for 7–10 days. VIMS susceptibility and Theta-band EEG phase synchronization were measured before and after the adaptation training. The results revealed that the inter-hemispheric connectivity in temporal-parietal regions not only significantly differed between the susceptible and resistant groups, but also increased with individual resistance enhancement. The strength of this connectivity was negatively correlated to individual level of VIMS symptoms. Machine learning models based on whole brain connection patterns effectively identified susceptible individuals and tracked changes in susceptibility following training. All effects were also observed in untrained stimulus type, indicating the robustness of the connectivity indicators. These findings underscore the importance of inter-hemispheric coordination in VIMS and highlight the potential of EEG phase synchronization as a tool for testing and monitoring individual susceptibility to VIMS.

Keywords Visually induced motion sickness · Inter-hemispheric connectivity · Adaptation training · EEG phase synchronization

✉ Yue Wei
yweiaj@connect.ust.hk

1 Department of Basic Psychology, School of Psychology, Shenzhen University, 3688 Nanhai Avenue, Nanshan District, Shenzhen 518060, China

2 HKUST-Shenzhen Research Institute, 9 Yuexing First Road, South Area, Hi-tech Park, Nanshan, Shenzhen 518057, China

3 Bio-Engineering Graduate Program, School of Engineering, The Hong Kong University of Science and Technology, Hong Kong, China

4 Department of Industrial Engineering and Decision Analytics, The Hong Kong University of Science and Technology, Hong Kong, China

5 Division of Neural Dynamics, Department of System Neuroscience, National Institute for Physiological Sciences, National Institutes of Natural Sciences, 38 Nishigonaka, Myodaiji, Okazaki, Aichi 444-8585, Japan

6 Physiological Sciences Program, Department of Advanced Studies, SOKENDAI, 38 Nishigonaka, Myodaiji, Okazaki, Aichi 444-8585, Japan

Abbreviations

BEH	Behavioral test
EEG	Electroencephalogram
ERP	Event-related potential
LOOCV	Leave-one-out cross validation
MT+	Medial temporal area including medial temporal (MT) and medial superior temporal (MST) areas
MSSQ	Motion sickness susceptibility questionnaire
MaxNausea	Maximum nausea score recorded during each exposure
PLV	Phase locking value
ROL	Roll rotation
PIT	Pitch rotation
RAN	Random motion
SSQ	Simulator sickness questionnaires
SVM	Support vector machine
LR	Logistic regression

VIMS	Visually induced motion sickness
VIMSres	VIMS-resistant
VIMSsus	VIMS-susceptible
VIMSSQ	Visually induced motion sickness susceptibility questionnaire
VIP	Ventral intraparietal area

Introduction

Visually induced motion sickness (VIMS), also known as cybersickness, is a common discomfort experienced by stationary viewers when exposed to visual motion (Golding et al. 2012; Keshavarz et al. 2015), with symptoms including disorientation, oculomotor disturbance, and nausea (Bruck and Watters 2011; Griffin 1990; Kennedy et al. 1993; Wang et al. 2021). VIMS poses a significant challenge to user experiences in virtual reality (VR) and large-screen movies (Hoshino 2012; Riecke 2011; Stanney et al. 1998). With the advancement and widespread use of VR technology, identifying and monitoring an individual's vulnerability to VIMS and customizing suitable user programs have become increasingly important (Bratosin et al. 2022; Kamińska et al. 2019; Rebenitsch and Owen 2021; Riecke 2011). However, current research has only focused on identifying neurological correlates that differ between groups. It is crucial to further investigate the neurological responses to individual susceptibility changes. Electroencephalography (EEG), with its portability, temporal and spatial resolution, is a promising tool for studying VIMS susceptibility (Keshavarz et al. 2015; Wei et al. 2023), which can also enable early prediction and intervention in various applications (Li et al. 2023).

The susceptibility to VIMS can vary greatly among individuals (Golding 2006; Golding et al. 2021; Guo et al. 2017; So et al. 1999; Wei et al. 2019), and adaptation training through repeated exposures is one of the most effective methods to reduce VIMS susceptibility (Besnard et al. 2021; Keshavarz and Golding 2022; Reason 1978). However, this process is time-consuming, and the effectiveness may not transfer to untrained stimuli. Currently, the underlying brain dynamics associated with VIMS susceptibility and its adaptation remain unclear. Understanding these brain dynamics should enable us to design and implement protocols to overcome both problems, thereby ensuring all viewers have positive experiences in VR situations.

The human brain integrates multisensory information, primarily visual and vestibular cues, to perceive self-motion (Fetsch et al. 2009; Zhao et al. 2023). Previous studies have identified several key brain regions (e.g. MT+, VIP) in the temporal and parietal regions of both hemispheres, which are responsible for integrating visual and vestibular self-motion information (Chen et al. 2011b; DeAngelis et al. 2017). According to the widely accepted sensory conflict theory (Reason 1978), VIMS can be triggered when the visual system receives information about self-motion while the individual is actually stationary, resulting in a conflict with information from vestibular systems (Keshavarz et al. 2015).

While previous studies have mainly focused on analyzing the correlation between local activity in specific brain regions and VIMS (Chang et al. 2013; Chelen et al. 1993; Chuang et al. 2016; Farmer et al. 2015; Li et al. 2023; Napadow et al. 2013; Sheehan et al. 2009; Wei et al. 2023), recent evidence suggests that dynamic connectivity between brain regions is more closely related to VIMS. As supported by new biologically realistic neural network models (Zhang et al. 2016, 2019), strong dynamic connectivity between key multisensory integration brain regions is critical for the integration of conflicting visual-vestibular information. Moreover, it has been revealed that strong connectivity to the temporal and parietal regions is associated with resistance to motion sickness (Sakai et al. 2022; Wei et al. 2019). And connectivity-based indicators can predict VIMS susceptibility better than local activities (Wei et al. 2019). Conversely, VIMS-susceptible individuals exhibit decreased inter-hemispheric synchronization between the bilateral temporal-parietal regions (Miyazaki et al. 2015).

However, the existing research has only explored neural correlates that differ between groups with varying levels of susceptibility to VIMS (Miyazaki et al. 2015; Wei et al. 2019, 2023). This problem encompasses several limitations. First, between-subject susceptibility differences may be confounded by various other individual difference factors, such as the intensity of experienced vection and previous visual experience (Keshavarz et al. 2015). Secondly, to further reveal the association between dynamic brain connectivity and VIMS, evidence is lacking regarding changes in the dynamic connectivity strength following manipulations of individual susceptibility. Hence, further investigating the neurological responses to individual susceptibility changes holds crucial theoretical and practical value. To address this gap, this study aims to examine changes in brain dynamics before and after individual susceptibility is enhanced through adaptation training.

A third limitation in previous studies is the use of only one visual stimulus (Miyazaki et al. 2015; Wei et al. 2019, 2023); it is possible that the identified EEG correlates may be specific to that particular stimulus. Identifying EEG correlates of VIMS that can generalize to different visual stimuli is crucial for gaining further insights into the mechanisms of adaptation training transfer and enhancing their practical applications. In this study, we designed two types of experimental stimuli involving different axis rotations,

specifically roll and pitch, which are known to frequently provoke VIMS (Lackner 2014; Lackner and DiZio 2006). One type of stimulus (roll) was used for adaptation training, while both types of stimuli (roll and pitch) were used to examine the association between brain dynamic connectivity and VIMS susceptibility. Participants with different susceptibilities were recruited. Based on their VIMS levels in response to VIMS-provoking stimuli, the participants were divided into two groups: the VIMS-susceptible (VIMSsus) group underwent training to manipulate their susceptibility and explore changes in EEG phase synchronization. The VIMS-resistant (VIMSres) group, serving as a control, also participated in the training. As EEG phase synchronization reflect brain dynamic connectivity associated with multimodal integration (Murray and Wallace 2011; Wei et al. 2019), this study accessed the degree of EEG phase synchronization to investigate pre- and post-training changes in the strength of inter-hemispheric connectivity between bilateral temporal-parietal regions. We tested three hypotheses, as follows.

(H1) Based on previous research (Miyazaki et al. 2015; Wei et al. 2019) and theoretical models (Zhang et al. 2019), we predict that the VIMSres group would exhibit stronger inter-hemispheric EEG phase synchronization between bilateral temporal-parietal regions compared to the VIMSsus group. (H2) We expected that changes in inter-hemispheric EEG phase synchronization would match VIMS susceptibility. Specifically: (H2a) For VIMSsus participants, we expected that, after adaptation training had reduced their VIMS susceptibility, inter-hemispheric EEG phase synchronization would increase. (H2b) For those in the VIMSres group who did not experience any changes in susceptibility, we anticipated that inter-hemispheric EEG phase synchronization would remain unchanged. (H3) Lastly, if neural correlates of individual VIMS susceptibility are insensitive to the type of visual stimulus, then inter-hemispheric EEG phase synchronization should be observed under both types of stimuli.

Methods

Participants

A total of 34 right-handed participants (age: 23.6 ± 3.3; male/females: 17/17) were recruited for the study after providing complete informed consent. All participants had 20/20 visual acuity or wore corrective lenses as necessary (Vision Tester: Stereo Optical CO. Inc. U.S.A., Model 2000). Prior to the experiment, participants completed the Motion Sickness Susceptibility Questionnaire (MSSQ, Golding, 1998) and the Visually Induced Motion Sickness Susceptibility Questionnaire – Short Version (VIMSSQ-short, Golding, 2019). They were instructed to abstain from alcohol and caffeine beverages for 10 h prior to the experiment. None of the participants had a history of heart disease, neurological diseases, or vestibular injury. Their participation was compensated with 50 HKD/hour. The study adhered to the ethical requirements set by the University Research Ethics Committee, in accordance with the Declaration of Helsinki. It received approval from the Human Participants Research Panel of the Hong Kong University of Science and Technology.

VIMS measures and grouping

To assess the VIMS response of participants to visual stimulations, participants were asked to score their nausea using a 7-point scale (ranging from 1= "no symptoms" to 7= "moderate nausea, want to stop"; see Online Appendix I.1, adopted from Golding and Kerguelen, 1992) at 5-minute intervals. The maximum nausea score recorded during each exposure was used as an indicator of the severity of nausea symptoms, referred to as MaxNausea. Additionally, participants completed Simulator Sickness Questionnaires (SSQ) before and after the visual motion exposure (pre-SSQ and post-SSQ), following the methodology proposed by Kennedy (1993).

The experiment comprised three stages: (1) pre-training, (2) training, and (3) post-training. All 34 participants completed the pre-training stage. Based on their reported MaxNausea levels during the exposure to two types of VIMS-provoking stimuli in the pre-training stage, participants were classified into two groups. Those reporting MaxNausea of 2 or less for both roll and pitch visual stimulations (indicating "no symptoms" or "slight unpleasant symptoms") were classified as VIMSres group ($n = 15$), while the remaining participants were classified as VIMSsus group ($n = 19$).

Due to personal scheduling conflicts, three participants from the VIMS-resistant group and two participants from the VIMS-susceptible group did not participate in the subsequent training stage. The training stage and the post-training stage was completed by the remaining 29 participants (age: 23.8 ± 3.3; male/female: 14/15). Both VIMS groups comprised a mixture of genders. There were no significant group differences in age. Table 1 summarizes information on VIMS susceptibility and demographic characteristics of participants in the two groups.

Table 1 Summary of the group information on VIMS susceptibility, demographic characteristics, and EEG data quality

	VIMSres group	VIMSsus group	*P*
Pre-training stage			
Number of participants	15	19	
Age (years)	23.33 ± 3.26	23.73 ± 3.43	0.404
Gender (male%)	60%	42.1%	
MSSQ	12.68 ± 12.32	26.23 ± 11.09	0.004**
BEH(ROL) MaxNausea	1.27 ± 0.46	4.11 ± 1.99	< 0.001***
BEH(PIT) MaxNausea	1.20 ± 0.41	3.32 ± 1.83	< 0.001***
EEG(ROL) valid epochs	119.93 ± 23.11	117.21 ± 25.11	0.747
EEG(PIT) valid epochs	107.80 ± 23.04	116.47 ± 25.81	0.316
Training stage			
Number of participants	12	17	
Trained participants	12	13	
Untrained participants	0	4	
Post-training stage			
Number of trained participants	12	13	
Age (years)	23.23 ± 3.63	23.83 ± 3.38	0.672
Gender (male%)	38.5%	58.3%	
BEH(ROL) MaxNausea	1.00 ± 0.00	1.62 ± 0.51	0.008**
BEH(PIT) MaxNausea	1.00 ± 0.00	1.12 ± 1.12	0.022*
EEG(ROL) valid epochs	117.25 ± 22.86	104.46 ± 19.95	0.149
EEG(PIT) valid epochs	114.25 ± 34.28	127.54 ± 33.72	0.339

*$p < 0.05$, **$p < 0.01$, ***$p < 0.001$. VIMSres: VIMS-resistant; VIMSsus: VIMS-susceptible; BEH: behavioral test; ROL: roll rotation stimulation; PIT: pitch rotation stimulation; MSSQ: Motion Sickness Susceptibility Questionnaire; MaxNausea: maximum nausea score recorded during each exposure. Unpaired Student's t-tests were applied to compare between groups; as for non-normal distributed rating scores, unpaired Wilcoxon signed-rank tests were employed. Noted that there were no differences between the VIMSsus and VIMSres groups in terms of age and the quality of EEG data, except for the significant difference in VIMS susceptibility

Experiment procedure

Pre-training stage

In the pre-training stage, the baseline EEG phase synchronization and VIMS susceptibility were measured under two types of VIMS-provoking stimulation: roll rotation (ROL) and pitch rotation (PIT). This stage consisted of two EEG test sessions, which included short visual motion exposures with breaks to prevent VIMS, and two behavioral test (BEH) sessions to assess VIMS susceptibility of participants with longer exposures (Fig. 1A).

To prevent fatigue and adaptation, EEG recordings were collected in separate sessions, with a 7-day interval between them (see Fig. 1A). The EEG sessions consisted of 14 blocks, with rest periods between blocks to minimize the impact of motion sickness symptoms on neurological responses (Wei et al. 2019; Wilkins 2016). Half of the blocks adopted ROL stimulation, while the other half adopted PIT stimulation. The order of ROL and PIT blocks was randomly assigned.

Each block comprised 12 trials. The block and trial procedure were the same as in previous EEG work on VIMS (Wei et al. 2019). Each trial started with a 3-second black screen, followed by a randomly moving random-dot pattern (RAN), another 3-second black screen, and a short exposure (up to 1 min) to coherent rotation stimulation (ROL or PIT) in a sequential order. Participants were trained to press a button when they perceived self-motion during the coherent rotation stimulation, following the protocol from previous studies (Wei et al. 2018, 2019, 2023). Upon button press, the coherent rotation stimulation continued for an additional 3 s (refer to Fig. 2B for illustration of EEG trial procedure).

Seven days after the EEG sessions, baseline VIMS levels for ROL and PIT stimulation were measured in two separate BEH sessions. The order of ROL and PIT sessions was randomly assigned for participants. Two BEH sessions were spaced in a 10-day interval to avoid adaptation (see Fig. 1A). In the BEH sessions, the actual VIMS susceptibility of participants was assessed through extended continuous exposures to VIMS-provoking stimulation, lasting up to 20 min. Participants had the option to end the exposure early if they experienced moderate nausea (MaxNausea = 7) and were unable to continue watching. During the exposure, participants were instructed to report their nausea scores every 5 min. Additionally, they filled out the SSQ before and after each exposure.

Training stage

Previous research has shown that adaptation training through repeated daily exposures to a VIMS-provoking stimulation can effectively reduce the subsequent VIMS response to that specific stimulation in susceptible individuals (Howarth and Hodder 2008a; Kennedy et al. 2000). In this research, adaptation training was conducted by subjecting participants to repeated BEH sessions of ROL stimulation over consecutive days. Similar to the pre-training stage, participants completed pre- and post-session SSQ, and their nausea scores were recorded every 5 min during each session. Participants were permitted to request a stop if they experienced moderate nausea, which was indicated by a MaxNausea score of 7.

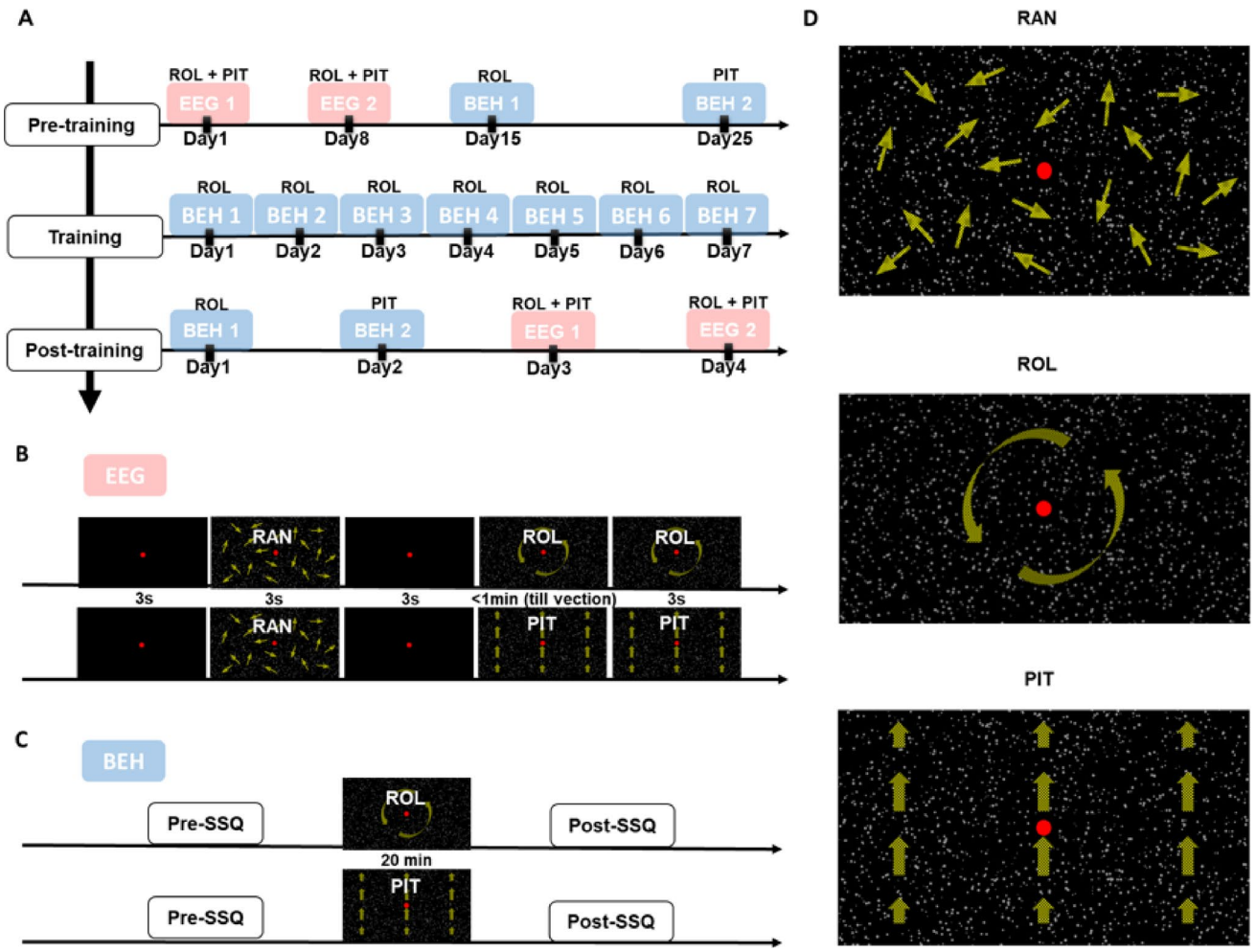

Fig. 1 Illustration of experimental procedures. **A** Stages of the experiment. **B** Trial procedure in a typical EEG session. **C** Procedures in BEH session. **D** Three types of visual motion stimuli used in the experiments. Arrows are added here to indicate the movement of dots but were not present in the experiments. BEH: behavioral test; ROL: roll visual stimulation; PIT: pitch rotation stimulation. Note that the order of ROL/PIT was randomly selected for each subject

The completion criteria for the adaptation training stage were as follows: (1) the MaxNausea scores reported by a participant in two consecutive sessions were both lower than 2, and (2) the participant had completed a minimum of 7 behavioral (BEH) sessions. Participants were allowed a maximum of 10 BEH sessions for training. If a participant's MaxNausea scores remained above 2 even after 10 sessions, they were considered to have failed to complete the adaptation training. These participants were placed in the "Untrained" group, while those who successfully completed the training were classified in the "Trained" group.

Post-training stage

In the post-training stage, the VIMS susceptibility and EEG phase synchronization were re-evaluated under two types of VIMS-provoking stimulation: ROL and PIT (see Fig. 1A for illustration). Two BEH sessions were conducted with a one-day interval between them. Similar to the pre-training stage, the order of ROL and PIT sessions was randomly assigned to participants. The SSQ and nausea scores were collected following the same procedure as in the pre-training stage.

After the BEH sessions, a follow-up experiment to analyze changes in EEG phase synchronization was conducted with a one-day interval. EEG recordings were obtained in separate sessions, with a one-day interval between them to avoid fatigue. Similar to the pre-training stage, the EEG session consisted of 14 blocks, with an equal number of ROL and PIT blocks. The order of ROL and PIT blocks was randomly assigned to participants. The EEG trial procedure was implemented in the same manner as in the pre-training stage.

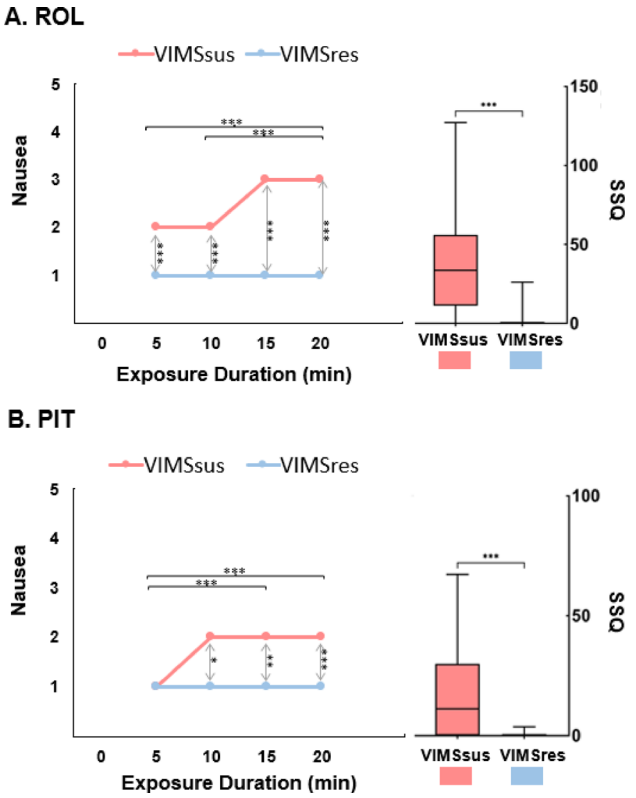

Fig. 2 Nausea and SSQ scores in pre-training stage of two VIMS groups under ROL and PIT condition. VIMSsus: VIMS-susceptible group (indicated by red color; $n=15$); VIMSres: VIMS-resistant group (indicated by blue color, $n=19$). Nausea score: nausea reported using a 7-point scale every 5 min. SSQ = post-SSQ – pre-SSQ (simulator sickness questionnaires rated after exposure, with the scores subtracted from those rated before exposure. Detail results of pre-/post-exposure SSQ are in Online Appendix I.2). ns: not significant; *$p<0.05$; **$p<0.01$; ***$p<0.001$. Wilcoxon signed-rank test was employed. **A** Reported nausea and SSQ scores of two groups under ROL (roll rotation stimulation) condition. **B** Reported nausea and SSQ scores of two groups under PIT (pitch rotation stimulation) condition

Visual motion stimuli

In this study, the visual stimuli consisted of grey dots with diameters ranging from 3.87 to 10.84 mm, which were displayed in random positions on a black background. There were three types of motion stimuli: coherent roll rotation (ROL), coherent pitch rotation (PIT), and random motion (RAN) (see Fig. 1D). In all motion conditions, approximately 1400 grey dots were visible on the screen. In the ROL condition, all grey dots rotated coherently in an anticlockwise direction around the center of the screen at an angular velocity of 32°/s, following the same approach as in previous work by Wei et al. (2019). In the PIT condition, all grey dots rotated around the pitch axis at the same velocity as in the ROL condition. In the RAN condition, similar randomly-positioned dots were used, but instead of rotating in a coherent manner, they moved linearly in random directions at the same tangential velocities as their counterparts in the ROL/PIT conditions (Brandt et al. 1998; Wei et al. 2019; Zhao 2017).

Apparatus and setups

The stimulations and EEG synchronization triggers used in the experiment were generated using Psychtoolbox-3 (Brainard 1997; Pelli 1997) with Matlab (version R2015b, academic license). The stimuli were displayed on a 65-inch OLED screen at a viewing distance of 50 cm, with a refresh rate of 60 Hz. The screen had a size of 1448 mm × 836 mm, providing a field of view of 114.17° × 79.79°. During the visual presentations, a black round disk area with a diameter of 10.84 cm (equivalent to 12.42°) and a red fixation point with a diameter of 5.42 mm (equivalent to 0.62°) were displayed at the center of the screen to ensure a stable fixation point for the participants. During the EEG sessions, participants were seated in front of the screen and were instructed to focus their gaze on the fixation point. A chin-rest was used to limit head and body movement in EEG sessions. In BEH sessions, participants also focused on the fixation point of the visual stimulation while standing. The screen was positioned at eye level in all sessions to ensure consistency.

The experiment was conducted inside an acoustic booth (a 1400-A-CT chamber custom-built by the Industrial Acoustics Company Limited). The metal wireframe of the booth provided electromagnetic shielding for the EEG electrodes, protecting them from background noise. The booth consisted of an inner and an outer compartment, with all computers placed in the outer compartment to minimize electrical interference. The OLED display was shielded with grounded wire mesh to further reduce potential interference. To eliminate visual distractions, we turned off all the lights and covered the TV and the participants with a large black curtain. This setup was consistent with previous studies conducted by Wei et al. (2018, 2019, 2023).

EEG collection and processing

During the experiment, EEG signals were collected using a DC-coupled NuAmps amplifier (Compumedics Neuroscan, 22 bits, monopolar). The amplifier was connected to 32-channel Ag/AgCl electrodes (Quik-Cap, Compumedics Neuroscan) that were placed on the participant's scalp according to the international 10–10 system referenced to linked mastoid electrodes. The impedance between each channel and the ground channel (AFz) was maintained below 10 kΩ. The raw EEG data were digitized at a sampling rate of 1000 Hz and with a bandwidth of DC-260 Hz.

EEG signal preprocessing

Prior to data analysis, a bandpass finite impulse response filter with a frequency range of 1.6–47 Hz was applied to remove unwanted frequencies and enhance the signal quality. Epochs corresponding to the different experimental conditions (ROL, PIT, RAN) were extracted from 2 s before the onsets to 3 s after the onsets. Then, epochs containing artifacts were excluded from further analysis. Artifact rejection was performed using the ERPLAB plugin within the EEGLAB toolbox. The moving-window peak-to-peak method was applied twice with different parameters (window size: 200 ms, step: 50 ms, threshold: ±100 μV; window size: 20 ms, step: 50 ms, threshold: ±50 μV). Epochs with extreme amplitudes exceeding ± 150 μV were also rejected. Table 1 is a summary of numbers of remaining valid EEG epochs. To further improve data quality, independent components analysis was applied to these remaining epochs. Artifactual components associated with blinking and eye movements were identified and removed by using an ICA-based procedure with the ADJUST plugin within EEGLAB (Mognon et al. 2011).To mitigate the effects of volume conduction, current source density analysis was performed at each electrode position on the cleaned epochs. This involved applying a spline interpolation with an order of 4 and a precision of 1.0e-5, following the method proposed in previous work (Kayser and Tenke 2006a, b).

Phase synchronization calculation

Wavelet analyses were performed to extract the instantaneous phase at each millisecond and at 1-Hz intervals with the central frequency ranging from 2 to 46 Hz, following previous works (Kawasaki et al. 2014; Lachaux, Jean-Philippe Rodriguez et al., 2000; Wei et al. 2019). The parameters used for the wavelet analysis were set as follows: $f/\sigma_f = 6$, where $\sigma_f = 1/(2\pi\sigma_t)$, and σ_t represents the standard deviation of the Gaussian window. To quantify the phase synchronization between the bilateral temporal and parietal regions, the phase locking value (PLV) was computed. In this work, the PLV analysis focused on the connections between inter-hemispheric pairs of electrodes placed over the temporal and parietal regions. Specifically, for the left hemisphere, we chose electrodes located in the temporal-parietal region, namely P3, P7, and TP7. In the right hemisphere, we selected symmetrical electrodes, namely P4, P8, and TP8 (see Fig. 4a). The PLV analysis was performed at each time point within the epoch between each pair of electrodes, following previous work. For a condition with N epochs, the PLV between electrode j and k, at time point t and frequency f was calculated as (Lachaux et al. 1999; Totah et al. 2013):

$$PLV_{j,k}(f,\ t)\ =\ N^{-1}\left|\sum e^{i\left[\varphi_j(t)-\varphi_k(t)\right]}\right|$$

Theta-band synchronization is commonly implicated in sensory conflict processing (Aitake et al., 2011a; Araújo et al., 2002; Jo et al., 2017; White et al., 2012) and has also been linked to the development of motion sickness (Chelen et al. 1993; Wei et al. 2019). Therefore, the present study also focused on theta-band phase synchronization, following previous experimental paradigms (Wei et al. 2019).

The dynamic time window representing the sensory conflict processing were determined following the methods described in previous work (Wei et al. 2019). Firstly, the node strength of each electrode was calculated by averaging all the PLV_z value of links connected to it. Then, the cluster-based permutation test (Maris and Oostenveld 2007) was adopted for both visual stimulations (ROL/PIT) to test the time points and electrodes demonstrating statistically significant difference with RAN conditions. Finally, the time period that was significantly higher than the RAN condition for both the ROL and PIT stimulus conditions was identified as the critical time window. The final PLV_z for each visual condition (ROL/PIT) was calculated by averaging the PLV_z across the identified critical time period.

Validations

The validation tests were performed to ensure the robustness and reliability of the results, accounting for small variations in epoch numbers. The Phase Locking Value (PLV) was transformed using Rayleigh's Z value to correct for the bias associated with the number of epochs (Totah et al. 2013). All analyses were repeated based on the Z-transformed PLV.

Machine learning models

To explore whether whole-brain EEG phase synchronization could help identify individuals susceptible to motion sickness and track changes in individual susceptibility. We trained two different machine learning models, Support Vector Machine (SVM) and logistic regression (LR), using the data from all 34 participants during the pre-training stage, across all visual stimuli. Because leave-one-out cross validation (LOOCV) is particularly useful for estimating the generalizability of classifiers, especially when the sample size is small (Pereira et al. 2009), this method was utilized to evaluate the performance of classifiers.

Since there are a total of 30 electrodes spaced over the whole head, forming 435 connection pairs, we employed forward feature selection, starting with the best-performing feature and gradually adding the most optimal feature at each step (the feature selection process is illustrated in Online Appendix I.3). The permutation test was used to

assess whether the accuracy values obtained were significantly higher than what would be expected by chance. The class labels (VIMSsus or VIMSres group) were randomly shuffled across the entire sample, and the classification procedure was repeated 5,000 times. The p-value for accuracy was determined by calculating the proportion of permutations that resulted in a higher value than the actual observed value in the real sample, divided by the total number of permutations (Cui et al. 2016).

Results

Baseline VIMS level in pre-training stage

In pre-training stage, the baseline VIMS level exhibited a similar pattern under both ROL and PIT conditions. Figure 2 provides an overview of the baseline VIMS levels for the VIMSsus and VIMSres groups, assessed during the long exposure (20-min) to VIMS provoking stimulation in BEH sessions. With increasing exposure to VIMS provoking stimulation, only the VIMSsus group demonstrated a significant increase in nausea score (Fig. 2). Moreover, the post-SSQ score of the VIMSsus group was significantly higher than their pre-SSQ score, indicating a significant post-exposure increase in MS symptom severity [Wilcoxon signed rank test, $p<0.001$]. In contrast, the VIMSres group maintained a consistently low level of nausea throughout the study, with no significant differences observed between their nausea scores (Fig. 2). Additionally, the SSQ score (post-SSQ – pre-SSQ) of VIMSsus group was found to be significantly higher than that of the VIMSres group [Wilcoxon signed rank test, $p<0.001$].

Table 1 presents the detailed mean and standard deviation values for MSSQ and MaxNausea scores in the BEH sessions for each group (VIMSsus/VIMSres) and visual condition (ROL/PIT). The MSSQ and MaxNausea scores of the VIMSsus group were significantly higher than those of the VIMSres group (see Table 1). These findings provide further support for the differential susceptibility to VIMS between the VIMSsus and VIMSres groups. Furthermore, the results confirmed that both visual stimulations (ROL, PIT) were capable of provoking VIMS in the susceptible group.

Adaptation training results

The training results are summarized in Table 1. In the training stage, a total of 25 participants, including 13 participants in the VIMSsus group, successfully completed the training and adapted to ROL stimulation (Trained = 25). Most trained participants completed the training within 7 sessions; while 3 VIMS-susceptible participants required additional exposure and satisfied the accomplishment criteria (one needed 9 training sessions training; another two needed 10 training sessions). In addition to the trained participants, there were 4 VIMS-susceptible participants who did not meet the criteria even after 10 training sessions. These untrained participants still experienced VIMS symptoms and nausea when exposed to ROL stimulation for 20 min after training (Untrained = 4). Figure 3a illustrates the change in MaxNausea scores of the trained participants over the course of 7 regular training sessions. The training profile and MaxNausea scores of all types of participants are in Online Appendix I.2.

All trained participants completed the post-training stage. Figure 3b and c present the MaxNausea scores for the pre-training and post-training stages, respectively, for the two trained VIMS groups (VIMSres and VIMSsus). In the ROL condition, both the MaxNausea scores [related samples Wilcoxon signed rank test, $p=0.003$] and SSQ (SSQ = post-SSQ – pre-SSQ) scores [related samples Wilcoxon signed rank test, $p=0.023$] of the VIMSsus group showed a significant reduction after training.

For the untrained visual stimuli, the results revealed that the training effects successfully transferred to the PIT condition in terms of nausea. The MaxNausea scores of the VIMSsus group showed a significant reduction after training [related samples Wilcoxon signed rank test, $p=0.016$]. For the overall symptoms measured by SSQ, although a decreasing trend was observed, the effects were not statistically significant ($p=0.151$). As for VIMSres group, no significant difference was found in MaxNausea and SSQ scores between the pre-training and post-training stages. The results confirmed that the VIMS susceptibility of trained VIMSsus participants was reduced after the training, while the VIMS susceptibility of the VIMSres group remained unchanged.

EEG phase synchronization results

Firstly, to identify the critical time window related to self-motion perception (Wei et al. 2019), we compared the averaged global PLV node strength between the random (RAN) condition and each rotation condition (ROL, PIT). A cluster-based permutation test was applied on the EEG datasets collected in the pre-training stage for each visual condition ($n=34$). For the ROL condition, a positive cluster was identified in the time window of 157-466ms [$p<0.001$] (Fig. 4B). For the PIT condition, a positive cluster was found in the time window of 181-341ms [$p=0.003$] (Fig. 4C). To enable a comparative analysis for different visual conditions, a critical time window of 181-341ms that overlapped with both the ROL and PIT conditions was selected. The PLV values within the critical time window were averaged

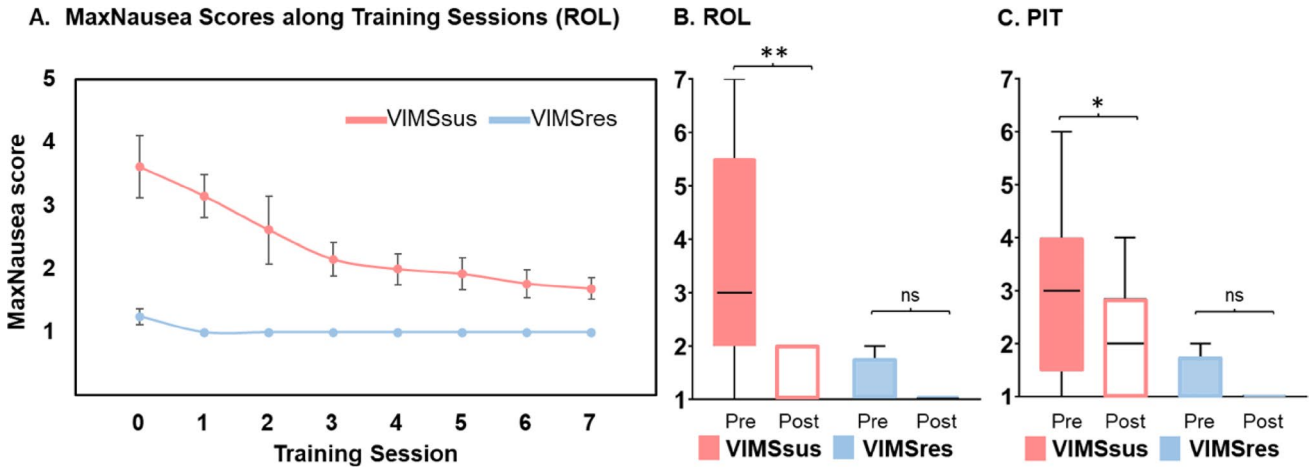

Fig. 3 Adaptation training results for trained participants. VIMSsus: VIMS-susceptible group (indicated by red color; $n=13$); VIMSres: VIMS-resistant group (indicated by blue color, $n=12$). MaxNausea: maximum nausea score recorded during each exposure. ns, not significant; ** $p<0.01$; * $p<0.05$. **A** Changes in MaxNausea scores reported by the two groups (showed with mean and std) of trained participants over the training sessions. Note that Session 0 corresponds to the results of the pre-training stage. **B** Box plot represents the MaxNausea scores for the trained participants from VIMSres and VIMSsus groups in the pre-training and post-training stages under the ROL (roll rotation) condition. **C** Box plot represents MaxNausea scores for the same two groups in the pre-training and post-training stages under the PIT (pitch rotation) condition. Note that the untrained participants, who were not the focus of this study, were not included in this figure but are shown in Online Appendix I.2 for clarity

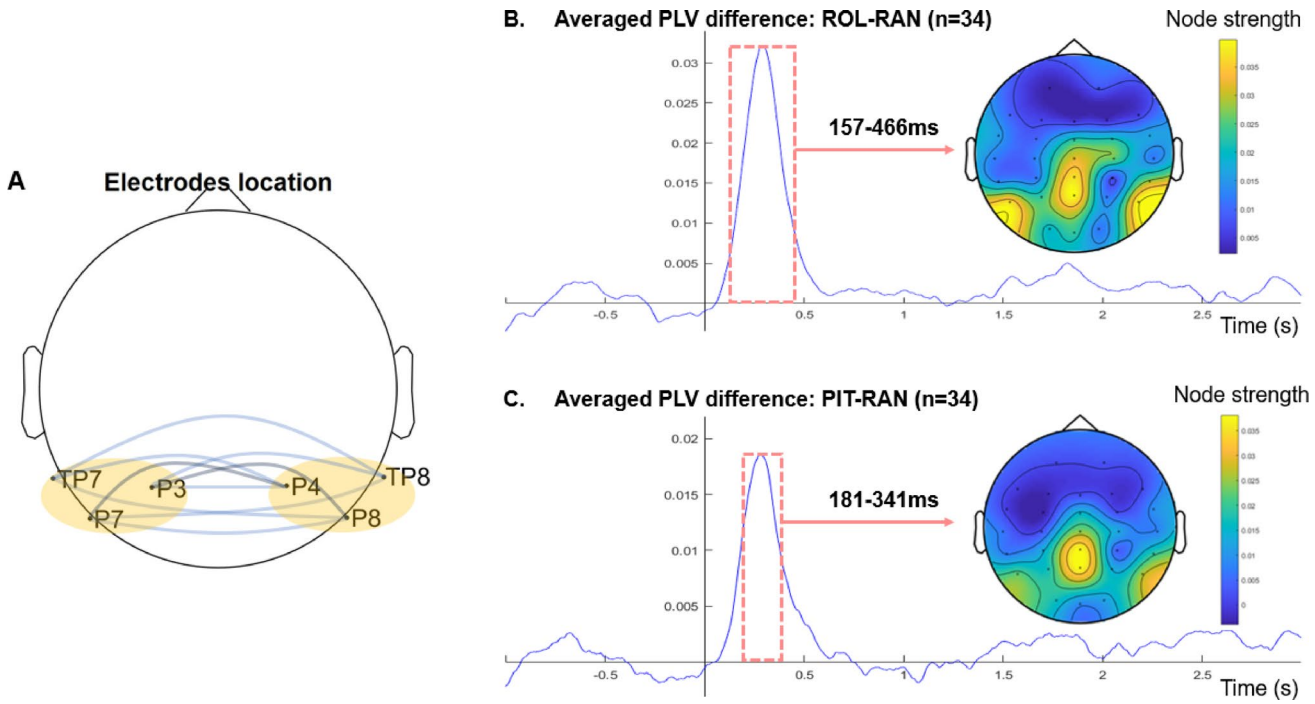

Fig. 4 Electrodes and critical time window for PLV indicator. **A** Positions of six selected electrodes on the scalp, located over the bilateral temporal-parietal regions. Nine inter-hemispheric connections formed by pairing these electrodes are indicated by dark blue lines. PLV was calculated for each of those connections. **B** Line graph showing difference of the averaged overall PLV of between ROL (roll rotation) and RAN conditions. The topography displays node strength distribution (averaged across window 154-466ms of the significant cluster). **C** Line graph showing difference of the averaged overall PLV of between PIT (pitch rotation) and RAN conditions. The topography displays node strength distribution (averaged across the window 181-341ms of the significant cluster)

for all connections of interest (see Fig. 4A) in each condition and for each participant for further analysis.

To examine the difference in inter-hemispheric EEG phase synchronization between the VIMSsus group and VIMSres group, independent sample t-tests were conducted for all connections of interest in each condition during the pre-training stage. For the ROL condition, the inter-hemispheric pair P4-P7 showed a significant difference after applying Bonferroni correction [$t(32)=3.673$, $p=0.001$, Cohen's $d=1.27$], with the VIMSres group exhibiting higher PLV values than the VIMSsus group. Similarly, for the PIT condition, the pair P4-P7 also showed a significant difference [$t(32)=2.866$, $p=0.007$, Cohen's $d=0.99$] in the same direction. No other connection of interest reached significance. These results indicated that the VIMSres group displayed stronger inter-hemispheric PLV values compared to the VIMSsus group, supporting H1.

To investigate the changes in this identified inter-hemispheric EEG phase synchronization after reducing VIMS susceptibility, paired-sample t-tests were conducted on the P4-P7 pair between the pre-training and post-training stages in each condition. Figure 5 depicts the averaged PLV values in the pre-training and post-training stages for the trained participants. For the ROL condition in the trained VIMSsus group, the PLV value significantly increased after training [$t(12)=3.217$, $p=0.007$, Cohen's $d=0.89$], with the post-training stage showing higher values than the pre-training stage. Similarly, for the PIT condition in the trained VIMSsus group, the PLV value also significantly increased after training [$t(12)=3.087$, $p=0.009$, Cohen's $d=0.86$]. No significant difference was observed before and after training in the VIMSres group. These results suggested that inter-hemispheric PLV values were enhanced when the susceptibility was reduced, supporting H2a. Additionally, this identified inter-hemispheric PLV value remained unchanged in VIMSres participants whose susceptibility was not affected by training, indicating that the effect was not caused by the training procedure itself (supporting H2b). Furthermore, these effects were observed for both types of visual stimuli (ROL and PIT), suggesting that this inter-hemispheric EEG phase synchronization was associated with general VIMS susceptibility rather than specific types of visual stimuli (supporting H3).

Predicting VIMS using EEG phase synchronization

To further explore the association between the identified PLV indicators and actual motion sickness symptoms, we calculated Spearman's rank correlation coefficients between PLV values and VIMS measures (MaxNausea and SSQ scores). Additionally, we included MSSQ and VIMSSQ-short for comparison with traditional scales. We found that during the pre-training stage, regardless of the ROL or PIT condition, the PLV values of the connection pair P4-P7 were

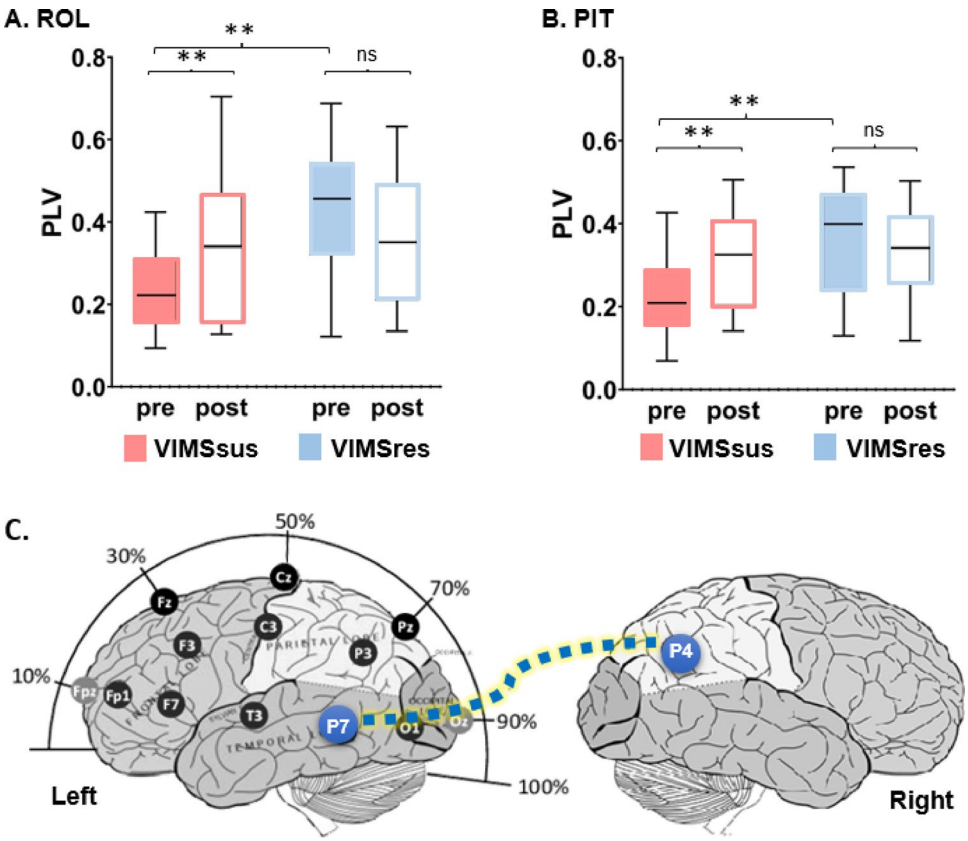

Fig. 5 Effects of training on inter-hemispheric EEG phase synchronization. VIMSsus: VIMS-susceptible group (indicated by red color; $n=13$); VIMSres: VIMS-resistant group (indicated by blue color, $n=12$). *** $p<0.001$, ** $p<0.01$, * $p<0.05$. **A** Under the ROL (roll rotation) condition, the PLV (Phase locking value) of the connection pair P4-P7 in the pre-training and post-training stages for the trained VIMS groups. **B** Under the PIT (pitch rotation) condition, the PLV values of the connection pair P4-P7 in the pre-training and post-training stages for the trained VIMS groups. **C** Illustration for the location of electrodes based on 10–10 system. The connection pair linking electrode P4 and P7 is highlighted by blue

significantly correlated with VIMS measures (see Table 2). In general, these coefficients were higher compared to traditional subjective VIMS susceptibility rating scales (MSSQ and VIMSSQ-short). No significant correlation was found in the post-training stage, possibly due to the reduced VIMS and limited symptoms reported by most participants in that stage.

Then, we further analyzed whether machine learning models (SVM, LR) can differentiate VIMSsus individuals based on PLV connections calculated across all electrode pairs placed over the entire brain. As the susceptibility of participants were modified through adaptation training, we also conducted additional tests to determine whether these models had the ability to recognize changes in susceptibility categories during the post-training stage. The participants were re-labeled using the same classification criteria as in the pre-training stage. Specifically, the 25 participants who were successfully trained were relabeled as the VIMSres group, while the untrained participants remained labeled as the VIMSsus group. Machine learning models were trained using additional data from one type of visual stimuli and evaluated using a different type of visual stimuli. Therefore, each model was tested using visual stimuli data in the post-training stage that it had not encountered before.

The results showed that the SVM and LR models achieved an accuracy of over 75% on both pre-training and post-training data. For the pre-training stage, the optimal feature size was approximately 40 for all models, while for the post-training stage, the optimal feature size was around 20 (see Online Appendix I.3). Overall, a smaller feature size was found to benefit the generalization of the models to post-training stage. Permutation tests revealed that the accuracy of all models was significantly higher than chance. Figure 6A displays the accuracy for the different models and the significance level of permutation tests under each condition with the optimal feature size. Figure 6C displays the positions on the scalp of the top 5 selected features of electrode pairs chosen by the forward feature selection. Among these features, the top two ranked electrode pairs were P4-Cpz and P4-P7. Additionally, all top 5 connections are linked to electrode P4 (Fig. 6C), indicating the importance of the right parietal region.

.

Table 2 Correlation between PLV values, traditional VIMS susceptibility scales and VIMS symptom levels in pre-training stage

	SSQ (ROL)	SSQ (PIT)	MaxNausea (ROL)	MaxNausea (PIT)
PLV_{P4-P7}(ROL)	−0.606** (p=0.001)	−0.494** (p=0.012)	−0.609** (p=0.001)	−0.399* (p=0.048)
PLV_{P4-P7} (PIT)	−0.546** (p=0.005)	−0.422* (p=0.035)	−0.589** (p=0.002)	−0.243 (p=0.242)
MSSQ	0.328 (p=0.110)	0.552** (p=0.004)	0.282 (p=0.172)	0.395 (p=0.051)
VIMSSQ-short	0.060 (p=0.775)	0.184 (p=0.378)	0.177 (p=0.398)	0.303 (p=0.141)

*p<0.05, **p<0.01, ***p<0.001. PLV_{P4-P7}: the averaged PLV value of electrode pair P4 and P7 across critical time window; ROL: roll rotation stimulation; PIT: pitch rotation stimulation; SSQ=post-SSQ – pre-SSQ. MaxNausea: maximum nausea score recorded during each exposure; MSSQ: Motion Sickness Susceptibility Questionnaire; VIMSSQ-short: Visually Induced Motion Sickness Susceptibility Questionnaire; Note that the table displays the Spearman's rank correlation coefficients (ρ) and the statistical significance (p-values) of the coefficients

Validation results

To account for potential effects of epoch size variation, all data processing was re-analyzed using Z-transformed PLV data. These re-analyses confirmed that all results remained robust and consistent with the main findings (see Online Appendix I.4 for details).

To validate the statistical power of current study, we conducted a post-hoc power analysis using the G*Power software(Faul et al. 2007) to obtain the power ($1-\beta$) of the tests supporting our hypotheses. Regarding H1, the results were supported by the significant independent sample t-tests between VIMSsus group and VIMSres group for ROL[$t(32)=3.673$, $p=0.001$, Cohen's $d=1.27$] and PIT [$t(32)=2.866$, $p=0.007$, Cohen's $d=0.99$] condition, the achieved power (1-β) calculated are 0.97 (ROL) and 0.88 (PIT). Regarding H2/H3, the results were paired-sample t-tests between the pre-training and post-training stages in trained participants for ROL [$t(12)=3.217$, $p=0.007$, Cohen's $d=0$ 0.89] and PIT [t (12)=3.087, $p=0.009$, Cohen's $d=0.86$] condition, the achieved statistical power ($1-\beta$) calculated are 0.92 and 0.90.

Discussion

This study utilized a combined cross-sectional and longitudinal experimental design. By manipulating adaptation training to reduce VIMS susceptibility in participants and comparing their EEG phase synchronization with that of the control counterparts, we aimed to thoroughly examine the association between inter-hemispheric connectivity of the bilateral temporal-parietal region and VIMS susceptibility. In this section we elaborate on three major topics: (a) cross-sectional evidence, (b) longitudinal evidence, and (c) the use of EEG phase synchronization for identifying susceptible individuals. Finally, some limitations and future directions are discussed.

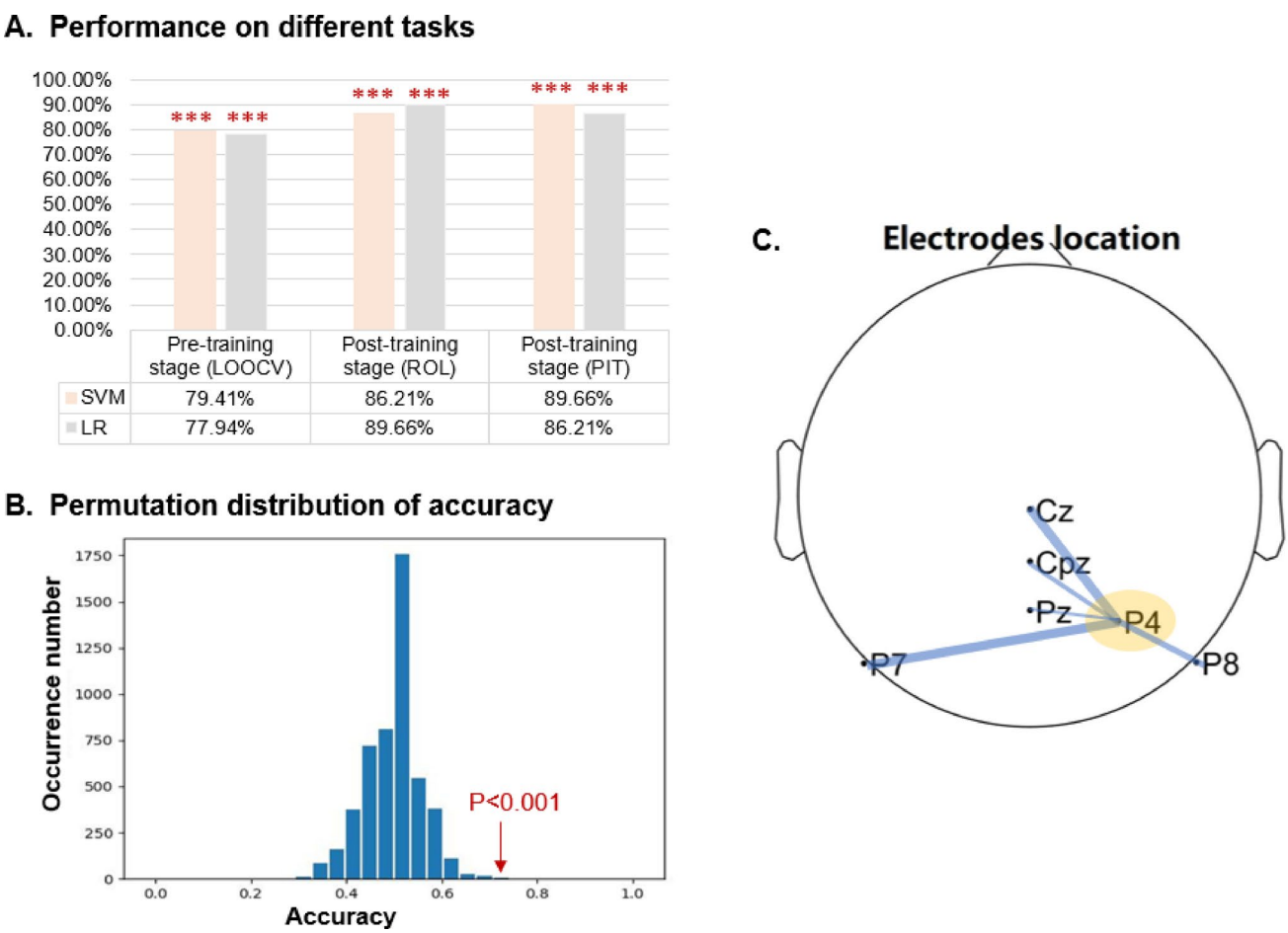

Fig. 6 Machine learning model performance and top features for identifying VIMS susceptibility. **A** Performance of the machine learning models (SVM and LR) evaluated on different tasks. All reported results were obtained using the optimal feature size for each specific model, which varied for different conditions (detailed in Online Appendix I.3). *** $p<0.001$ for comparison with chance. The pre-training stage involved training the models in two visual conditions and evaluating them using LOOCV. In the post-training stage, the models were trained on additional data from one visual stimulus type and evaluated on another type. **B** Histogram of the permutation distribution of accuracy. The arrow indicates the accuracy value that achieved a significant p-value of 0.001. **C** The diagram displays the top five connection pair features selected through forward feature selection using pre-training stage data. The thickness of the connecting lines indicates feature importance, with thicker lines representing earlier selection. All important features are connected to P4, highlighted by a yellow circle

Cross-sectional results: vimssus group exhibited weaker functional connectivity

Results from the pre-training stage indicated that the VIMSsus group showed weaker dynamic functional connectivity in the bilateral temporal-parietal region when exposed to VIMS-provoking stimuli compared to the VIMSres group. These findings are consistent with previous research comparing susceptible and resistant individuals. For example, Wei et al. (2019) found impaired EEG theta-band phase synchronization to the temporal and parietal region in VIMS-susceptible individuals under similar visual motion stimulation. Previous MRI studies have found that both resting-state functional connectivity and structural connectivity strength in the parietal region are associated with motion sickness susceptibility (Sakai et al. 2022). Another fMRI study found desynchronization in the bilateral temporal-parietal region of a VIMS-susceptible group during VIMS-provoking stimuli (Miyazaki et al. 2015). Overall, these findings suggest that VIMSsus individuals have weaker functional connectivity involving the temporal-parietal regions, indicating reduced dynamic coordination in processing VIMS-provoking stimuli compared to VIMSres individuals.

Longitudinal results: Co-variation of VIMS susceptibility and functional connectivity

Importantly, this study further longitudinally compared changes in EEG phase synchronization levels in the trained

VIMSres group before and after adaptation training. This comparison aims to provide stronger novel evidence of the association between VIMS susceptibility and brain functional connectivity strength. Given our focus on inter-hemispheric connectivity, we examined the long-range connectivity link (electrode pair P4-P7) identified in the pre-training stage. We found that the dynamic connectivity between electrodes P4-P7 was not only weaker in the VIMS-susceptible population but also significantly enhanced after they exhibited improved resistance to VIMS through adaptation training. Furthermore, for the VIMSres group, whose susceptibility did not significantly change, connectivity remained stable. These findings provide dual support for the notion that the dynamic connectivity strength between electrodes P4-P7 is associated with VIMS susceptibility rather than the training process or inherent differences among specific groups.

Functional substrates underlying P4–P7 connectivity in MS

The response of the P4 channel to visual motion stimulation likely reflects neural activity in the right VIP and right temporoparietal junction (TPJ). Both VIP and TPJ are considered key nodes in the vestibular processing network and also receive input from visual motion signals (Chen et al. 2011b; DeAngelis et al. 2017; Smith et al. 2017; Wall and Smith 2008). This is supported by previous human EEG and fNIRS studies, which have shown that channels around P4 respond to both vestibular (Zhao et al. 2023) and visual motion stimuli (Dowsett et al. 2020; Keshavarz and Berti 2014; Vilhelmsen et al. 2015; Yeo et al. 2024). Although multiple cortical regions are involved in visuo-vestibular multisensory integration, the right parietal cortex appears to also play a particularly central role in processing self-motion conflicts (Sakai et al. 2022). Its activation strength has been closely associated with motion sickness severity (Yeo et al. 2024).

As for P7, based on prior research, the activity at this electrode likely reflects neural responses from the left MT+area (Scrivener and Reader 2022), which is a key region within the visual motion processing network that also receives vestibular inputs (Britten 2008; Chen et al. 2011a; DeAngelis et al. 2017; Gu et al. 2008). While the activation strength of MT+itself may not be directly associated with motion sickness (MS), previous studies have shown that functional connectivity involving MT+, particularly long-range inter-hemispheric connections (Miyazaki et al. 2015), is negatively associated with MS susceptibility—i.e., weaker or fewer such connections are linked to higher susceptibility (Wei et al. 2019).

Therefore, the dynamic P4–P7 connectivity identified in this study may reflect interhemispheric communication between two multisensory integration centers—the right VIP and the left MT+. According to the decentralized multisensory integration model (Zhang et al. 2016, 2019), such centers are not functionally redundant but serve as distributed nodes that collectively support optimal information integration. Stronger dynamic connectivity between these regions may promote the resolution of conflicting sensory cues by supporting consistent and coherent multisensory representations (Zhang et al. 2019). In contrast, weaker connectivity may lead to the segregation of sensory signals and inconsistent responses between the processing centers of visual and vestibular modalities (e.g., VIP and MT+), contributing to unresolved sensory conflicts and increased susceptibility to motion sickness.

Potential of EEG phase synchronization for identifying susceptible individuals

In this study, participants were trained using roll rotation stimuli, and the results showed that the effectiveness of enhancing VIMS resistance successfully transferred to untrained pitch rotation stimuli. Following the training, participants reported a significant decrease in the severity of nausea specifically in response to the untrained pitch stimuli. Importantly, despite not being involved in the training, EEG phase synchronization obtained under the pitch condition showed enhancement after the training. This not only confirms that this study identified PLV indicators that are insensitive to stimulus type but also rules out the possibility that these connectivity changes are simply due to visual habituation.

In addition, the strengths of identified PLV indicators under both types of stimuli were closely related to the severity of individual motion sickness symptoms. This further supports the association between the strength of dynamic inter-hemispheric connections and VIMS susceptibility, confirming that PLV indicators derived from EEG data could serve as objective measures for screening individuals prone to motion sickness.

Indeed, EEG data can be used to train VIMS-predicting models. Specifically, machine learning models trained with whole-brain EEG phase synchronization connectivity strength can effectively identify susceptible individuals, even track their susceptibility changes. By incorporating data from a specific type of visual stimuli, these models can effectively identify the susceptibility to VIMS in individuals during the post-training stage, using data from novel visual stimuli. Interestingly, the EEG phase synchronization connection features selected by the classifier (Fig. 6) are consistent with our hypotheses regarding inter-hemispheric connections. The feature selection results also underscore the importance of the identified inter-hemispheric PLV

indicator (P4-P7). Furthermore, the results highlight the strong association between EEG phase connections involving the right parietal region and vulnerability to VIMS. This aligns with previous research, which discovered that the global connectivity to the right temporal-parietal region under VIMS-proving stimulation has the ability to predict an individual's MSSQ scores (Wei et al. 2019). Recent MRI research has also confirmed a strong correlation between VIMS and the global functional during resting state and structural connectivity to the parietal region (Sakai et al. 2022).

In summary, these findings emphasize the value of EEG in objectively identifying susceptibility to VIMS. The advantage lies in the shorter trial time required for analyzing PLV indicators, without the need for participants to experience motion sickness symptoms. This approach can be particularly useful for early identification of susceptible individuals and monitoring the occurrence of VIMS in specialized tasks (e.g., operating unmanned devices) before symptoms arise. It is worth mentioning that this study has confirmed that when the training effect successfully transfers to untrained novel stimuli, the EEG phase synchronization detected using the new stimuli also significantly enhances. This provides valuable neural evidence and a theoretical basis for designing better training processes in the future, monitoring training, and validating the transfer effects.

Limitations and future directions

This study primarily focused on the inter-hemispheric connections between the temporal and parietal regions. In the analysis, we discovered that other EEG phase connections involving the right parietal region are also closely related to VIMS susceptibility. These findings, together with previous results (Wei et al. 2019; Sakai et al. 2022), suggest a potential hub role of the right parietal region in resolving VIMS-related conflicts. Future work incorporating graph-theoretical approaches and evaluating global network properties would be valuable for further elucidating the network-level implications of these findings.

This work primarily examined participants who were trainable through repeated exposure to VIMS-provoking stimulation. Interestingly, we noticed that some participants did not show a decrease in susceptibility during the training, which is consistent with findings from previous studies where a minority of susceptible individuals did not respond to adaptation training (Howarth and Hodder 2008b; Regan 1995). In follow-up analysis, non-trainable participants showed a non-significant trend toward higher baseline PLV under PIT stimuli ($p=0.085$), and no significant change after training ($p=0.668$). This may suggest that their VIMS susceptibility involves factors not addressed by the current training protocol. Given the limited sample size, further studies with larger cohorts are needed to clarify these differences and potentially uncover distinct neural mechanisms.

Although the calculated statistical power for the main analyses exceeded 0.8, suggesting acceptable robustness, we acknowledge that the current results were based on a limited sample of university students. This may restrict the statistical power and generalizability of the findings, and further validation with a larger and more diverse sample is desirable. Moreover, it is important to note that non-visual factors, such as vestibular sensitivity and proprioceptive integration, may also contribute to individual differences in VIMS susceptibility. These factors were not systematically measured in the current study, which may limit the specificity of our conclusions. Future research should consider assessing vestibular function through tests like caloric or rotary chair stimulation, and proprioceptive integration via balance or joint position sense tasks. Controlling for these variables will help more precisely isolate the neural mechanisms underlying VIMS.

Conclusion

This study is the first investigation to utilize adaptation training and discover that functional brain connectivity strengthens as susceptibility to VIMS decreases. The findings emphasize the significant association between VIMS susceptibility and inter-hemispheric connectivity strength in the temporal and parietal regions. Of great importance, the study demonstrates that EEG phase synchronization indicators can be used to identify VIMS susceptibility. The connectivity strength patterns of EEG phase synchronization not only enable identification of individuals susceptible to VIMS but also facilitate tracking of individual susceptibility changes. Future work could explore real-time monitoring of individual susceptibility changes in motion sickness using EEG, potentially through portable or wearable systems. Such approaches could contribute to the prevention, detection, and mitigation of VIMS.

Supplementary Information The online version contains supplementary material available at https://doi.org/10.1007/s11571-025-10354-7.

Acknowledgements The authors would like to thank the National Natural Science Foundation of China under project No. 32200923 and Shenzhen Science and Technology Innovation Committee for partially supporting the work via project No. 20220810172237002, No. 20231124100927001 and project JCYJ20170413173515472 (SZSZSTI1731). The study was also partially supported by the Hong Kong Research Grants Council through HKUST16200915.

Author contributions Yixuan W. (Yixuan WANG) executed the experiments, performed the data analysis, and participated in drafting

the manuscript. Yue.W. (Yue WEI) participated in the experimental design, data analysis, statistical analysis, and writing the manuscript. Yue W. and R.S. (Richard H. Y. SO) secured funding for the project. Yixuan W. and R.S. were also involved in the design of the experiments. Yue W., K.K.(Keiichi KITAJO) and Y.O. (Yuka O. OKAZAKI) were involved in the data and statistical analysis of the data. Yue W. was responsible for the overall coordination and ensured the integrity of the research. All authors reviewed and revised the manuscript.

Data availability No datasets were generated or analysed during the current study.

Declarations

Competing interests The authors declare no competing interests.

References

Aitake M, Hori E,Matsumoto J, Umeno K, Fukuda M, Ono T, Nishijo H (2011a) Sensory mismatch inducesautonomic responses associated with hippocampal theta waves in rats. Behav Brain Res 220:244–253. https://doi.org/10.1016/j.bbr.2011.02.011

Araújo DB de, Baffa O, Wakai RT (2002) Theta oscillations and human navigation: a magnetoencephalography study. J Cogn Neurosci 14:70–78. https://doi.org/10.1162/089892902317205339

Besnard S, Bois J, Hitier M, Vogt J, Laforet P, Golding JF (2021) Motion sickness lessons from the Southern Ocean. Aerosp Med Hum Perform. https://doi.org/10.3357/AMHP.5696.2021

Brainard DH (1997) The psychophysics toolbox. Spat Vis 10(4):433–436. https://doi.org/10.1163/156856897X00357

Brandt T, Bartenstein P, Janek A, Dieterich M (1998) Reciprocal inhibitory visual-vestibular interaction. Visual motion stimulation deactivates the parieto-insular vestibular cortex. Brain 121(9):1749–1758

Bratosin IA, Pavaloiu IB, Goga N, Luca AI (2022) Virtual reality application for pain management: user requirements. Int J Adv Comput Sci Appl 13(4). https://doi.org/10.14569/IJACSA.2022.0130441

Britten KH (2008) Mechanisms of self-motion perception. Annu Rev Neurosci 31:389–410. https://doi.org/10.1146/annurev.neuro.29.051605.112953

Bruck S, Watters PA (2011) The factor structure of cybersickness. Displays 32(4):153–158. https://doi.org/10.1016/J.DISPLA.2011.07.002

Chang E, Hwang I, Jeon H, Chun Y, Kim HT, Park C (2013) Effects of rest frames on cybersickness and oscillatory brain activity. 2013 Int Winter Workshop Brain-Computer Interface BCI 2013 62–64. https://doi.org/10.1109/IWW-BCI.2013.6506631

Chelen WE, Kabrisky M, Rogers SK (1993) Spectral analysis of the electroencephalographic response to motion sickness. Aviat Space Environ Med 64(1):24–29

Chen A, DeAngelis GC, Angelaki DE (2011a) Convergence of vestibular and visual self-motion signals in an area of the posterior Sylvian fissure. J Neurosci 31(32):11617–11627. https://doi.org/10.1523/JNEUROSCI.1266-11.2011

Chen A, DeAngelis GC, Angelaki DE (2011b) Representation of vestibular and visual cues to self-motion in ventral intraparietal cortex. J Neurosci 31(33):12036–12052. https://doi.org/10.1523/JNEUROSCI.0395-11.2011

Chuang S, Chuang C, Yu Y, King J, Lin C (2016) EEG alpha and gamma modulators mediate motion sickness-related spectral responses. Int J Neural Syst 1650007. https://doi.org/10.1142/S0129065716500076

Cui Z, Xia Z, Su M, Shu H, Gong G (2016) Disrupted white matter connectivity underlying developmental dyslexia: a machine learning approach. Hum Brain Mapp 37(4):1443–1458. https://doi.org/10.1002/hbm.23112

DeAngelis GC, Greenlee MW, Angelaki DE, Smith AT (2017) Distributed visual–vestibular processing in the cerebral cortex of man and macaque. Multisens Res. https://doi.org/10.1163/22134808-00002568

Dowsett J, Herrmann CS, Dieterich M, Taylor PCJ (2020) Shift in lateralization during illusory self-motion: EEG responses to visual flicker at 10 hz and frequency-specific modulation by tACS. Eur J Neurosci 51(7):1657–1675. https://doi.org/10.1111/EJN.14543

Farmer AD, Ban VF, Coen SJ, Sanger GJ, Barker GJ, Gresty MA, Giampietro VP, Williams SC, Webb DL, Hellström PM, Andrews PLR, Aziz Q (2015) Visually induced nausea causes characteristic changes in cerebral, autonomic and endocrine function in humans. J Physiol 593(5):1183–1196. https://doi.org/10.1113/jphysiol.2014.284240

Faul F, Erdfelder E, Lang AG, Buchner A (2007) G*Power 3: A flexible statistical power analysis program for the social, behavioral, and biomedical sciences. Behav Res Methods 39(2):175–191. https://doi.org/10.3758/BF03193146/METRICS

Fetsch CR, Turner AH, DeAngelis GC, Angelaki DE (2009) Dynamic reweighting of visual and vestibular cues during self-motion perception. J Neurosci 29(49):15601–15612. https://doi.org/10.1523/JNEUROSCI.2574-09.2009

Golding JF (1998) Motion sickness susceptibility questionnaire revised and its relationship to other forms of sickness. Brain Res bulletin 47(5):507-516

Golding JF (2006) Motion sickness susceptibility. Auton Neurosci 129(1–2):67–76. https://doi.org/10.1016/j.autneu.2006.07.019

Golding J, Kerguelen M (1992) Acomparison of the nauseogenic potential of low-frequency vertical versus horizontal linearoscillation. Aviation, space, Environ medicine 63(6):491–497

Golding JF, Doolan K, Acharya A, Tribak M, Gresty MA (2012) Cognitive cues and visually induced motion sickness. Aviat Space Environ Med 83(5):477–482. https://doi.org/10.3357/ASEM.3095.2012

Golding JF, Ra A, Keshavarz B (2021) Predicting individual susceptibility to visually induced motion sickness by questionnaire. 2(February):1–11. https://doi.org/10.3389/frvir.2021.576871

Griffin MJ (1990) Handbook of human vibration. Academic

Gu Y, Angelaki DE, DeAngelis GC (2008) Neural correlates of multisensory cue integration in macaque MSTd. Nat Neurosci 11(10):1201–1210. https://doi.org/10.1038/nn.2191

Guo CCT, Chen DJZ, Wei IY, So RHY, Cheung RTF (2017) Correlations between individual susceptibility to visually induced motion sickness and decaying time constant of after-nystagmus. Appl Ergon 63:1–8. https://doi.org/10.1016/j.apergo.2017.03.011

Hoshino O (2012) Regulation of ambient GABA levels by neuron-glia signaling for reliable perception of multisensory events. Neural Comput 24(11):2964–2993. https://doi.org/10.1162/NECO_a_00356

Howarth PA, Hodder SG (2008a) Characteristics of habituation to motion in a virtual environment. Displays 29(2):117–123. https://doi.org/10.1016/j.displa.2007.09.009

Howarth PA, Hodder SG (2008b) Characteristics of habituation to motion in a virtual environment. Displays 29(2):117–123. https://doi.org/10.1016/j.displa.2007.09.009

Jo H-G, Malinowski P, Schmidt S (2017) Frontal theta dynamics during response conflict in long-term mindfulness meditators. Front Hum Neurosci 11:299. https://doi.org/10.3389/fnhum.2017.00299

Kamińska D, Sapiński T, Wiak S, Tikk T, Haamer RE, Avots E, Helmi A, Ozcinar C, Anbarjafari G (2019) Virtual reality and its

applications in education: survey. Information. https://doi.org/10.3390/info10100318
Kawasaki M, Kitajo K, Yamaguchi Y (2014) Fronto-parietal and fronto-temporal theta phase synchronization for visual and auditory-verbal working memory. Front Psychol 5(MAR):200. https://doi.org/10.3389/fpsyg.2014.00200
Kayser J, Tenke CE (2006a) Principal components analysis of laplacian waveforms as a generic method for identifying ERP generator patterns: I. evaluation with auditory oddball tasks. Clin Neurophysiol 117(2):348–368. https://doi.org/10.1016/j.clinph.2005.08.034
Kayser J, Tenke CE (2006b) Principal components analysis of laplacian waveforms as a generic method for identifying ERP generator patterns: II. Adequacy of low-density estimates. Clin Neurophysiol 117(2):369–380. https://doi.org/10.1016/j.clinph.2005.08.033
Kennedy RS, Lane NE, Berbaum KS, Lilienthal MG (1993) Simulator sickness questionnaire: an enhanced method for quantifying simulator sickness. Int J Aviat Psychol 3(3):203–220. https://doi.org/10.1207/s15327108ijap0303_3
Kennedy RS, Stanney KM, Dunlap WP (2000) Duration and exposure to virtual environments: sickness curves during and across sessions. Presence Teleoperators Virtual Environ 9(5):463–472. https://doi.org/10.1162/105474600566952
Keshavarz B, Berti S (2014) Integration of sensory information precedes the sensation of vection: a combined behavioral and event-related brain potential (ERP) study. Behav Brain Res 259:131–136. https://doi.org/10.1016/j.bbr.2013.10.045
Keshavarz B, Saryazdi R, Campos JL, & Golding JF (2019) Introducing the VIMSSQ: Measuring susceptibility to visually induced motion sickness. In Proceedings of the Human Factors and Ergonomics Society Annual Meeting 63(1):2267–2271. Sage CA: Los Angeles, CA: SAGE Publications
Keshavarz B, Golding JF (2022) Motion sickness: current concepts and management. Curr Opin Neurol 35(1):107–112. https://doi.org/10.1097/WCO.0000000000001018
Keshavarz B, Riecke BE, Hettinger LJ, Campos JL (2015) Vection and visually induced motion sickness: how are they related? Front Psychol 6:472. https://doi.org/10.3389/fpsyg.2015.00472
Lachaux JP, Rodriguez E, Martinerie J, Varela FJ (1999) Measuring phase synchrony in brain signals. Hum Brain Mapp 8(4):194–208
Lachaux J-P, Rodriguez E, Le van Quyen M, Lutz A, Martinerie J, Varela FJ (2000) Studying Single-Trials of phase synchronous activity in the brain. Int J Bifurcat Chaos 10(10):2429–2439. https://doi.org/10.1142/S0218127400001560
Lackner JR (2014) Motion sickness: more than nausea and vomiting. Exp Brain Res 232(8):2493–2510. https://doi.org/10.1007/s00221-014-4008-8
Lackner JR, DiZio P (2006) Space motion sickness. Exp Brain Res 175(3):377–399. https://doi.org/10.1007/S00221-006-0697-Y/FIGURES/4
Li G, Wang YK, McGill M, Pohlmann K, Brewster S, Pollick F (2023) Resting-state EEG in the vestibular region can predict motion sickness induced by a motion-Simulated in-car VR platform. 2023 IEEE Symp Ser Comput Intell SSCI 2023 47–52. https://doi.org/10.1109/SSCI52147.2023.10371953
Maris E, Oostenveld R (2007) Nonparametric statistical testing of EEG- and MEG-data. J Neurosci Methods 164(1):177–190. https://doi.org/10.1016/j.jneumeth.2007.03.024
Miyazaki J, Yamamoto H, Ichimura Y, Yamashiro H, Murase T, Yamamoto T, Umeda M, Higuchi T (2015) Inter-hemispheric desynchronization of the human MT+during visually induced motion sickness. Exp Brain Res. https://doi.org/10.1007/s00221-015-4312-y
Mognon A, Jovicich J, Bruzzone L, Buiatti M (2011) Adjust: an automatic EEG artifact detector based on the joint use of spatial and temporal features. Psychophysiology 48(2):229–240. https://doi.org/10.1111/j.1469-8986.2010.01061.x
Murray M, Wallace M (2011) The neural bases of multisensory processes. 20115459. https://doi.org/10.1201/b11092
Napadow V, Sheehan JD, Kim J, Lacount LT, Park K, Kaptchuk TJ, Rosen BR, Kuo B (2013) The brain circuitry underlying the temporal evolution of nausea in humans. Cereb Cortex (New York N Y : 1991) 23(4):806–813. https://doi.org/10.1093/cercor/bhs073
Pelli DG (1997) The videotoolbox software for visual psychophysics: transforming numbers into movies. Spat Vis 10(4):437–442. https://doi.org/10.1163/156856897X00366
Pereira F, Mitchell T, Botvinick M (2009) Machine learning classifiers and fMRI: a tutorial overview. Neuroimage 45(1):S199. https://doi.org/10.1016/j.neuroimage.2008.11.007
Reason T J (1978) Motion sickness adaptation: a neural mismatch model. J R Soc Med 71(11):819–829. http://www.pubmedcentral.nih.gov/articlerender.fcgi?artid=1436193&tool=pmcentrez&rendertype=abstract
Rebenitsch L, Owen C (2021) Estimating cybersickness from virtual reality applications. Virtual Reality 25(1):165. https://doi.org/10.1007/s10055-020-00446-6
Regan EC (1995) Some evidence of adaptation to immersion in virtual reality. Displays 16(3):135–139. https://doi.org/10.1016/0141-9382(96)81213-3
Riecke BE (2011) *Virtual Reality* (J.-J. Kim, Ed.). InTech. https://doi.org/10.5772/553
Sakai H, Harada T, Larroque SK, Demertzi A, Sugawara T, Ito T, Wada Y, Fukunaga M, Sadato N, Laureys S (2022) Left parietal involvement in motion sickness susceptibility revealed by multimodal magnetic resonance imaging. Hum Brain Mapp 43(3):1103–1111. https://doi.org/10.1002/hbm.25710
Scrivener CL, Reader AT (2022) Variability of EEG electrode positions and their underlying brain regions: visualizing gel artifacts from a simultaneous EEG-fMRI dataset. Brain Behav. https://doi.org/10.1002/brb3.2476
Sheehan J, LaCount L, Kim J, Lee J, John S, Newman S, Foy C, Michalek W, Park K, Kuo B, Napadow V, Lic A (2009) Neural correlates of motion sickness induced nausea - an fMRI study. Neuroimage 47:84. https://doi.org/10.1016/S1053-8119(09)70620-2
Smith AT, Beer AL, Furlan M, Mars RB (2017) Connectivity of the cingulate sulcus visual area (CSv) in the human cerebral cortex. Cereb Cortex (New York N Y : 1991). https://doi.org/10.1093/cercor/bhx002
So RHY, Finney CM, Goonetilleke RS (1999) Motion sickness susceptibility and occurrence in Hong Kong Chinese. Contemporary Ergonomics, Taylor & Francis
Stanney KM, Mourant RR, Kennedy RS (1998) Human factors issues in virtual environments: a review of the literature. Presence Teleoperators Virtual Environ 7(4):327–351. https://doi.org/10.1162/105474698565767
Totah NKB, Jackson ME, Moghaddam B (2013) Preparatory attention relies on dynamic interactions between prelimbic cortex and anterior cingulate cortex. Cereb Cortex 23(3):729–738. https://doi.org/10.1093/cercor/bhs057
Vilhelmsen K, van der Weel FR, Ruud, van der Meer ALH (2015) A high-density EEG study of differences between three high speeds of simulated forward motion from optic flow in adult participants. *Frontiers in Systems Neuroscience*, *9*. https://doi.org/10.3389/fnsys.2015.00146
Wall MB, Smith AT (2008) The representation of egomotion in the human brain. Curr Biology: CB 18(3):191–194. https://doi.org/10.1016/j.cub.2007.12.053
Wang Y, Du B, Wei Y, So RHY (2021) Visually induced roll circular vection: do effects of stimulation velocity differ for supine and

upright participants? Front Virtual Real 0:43. https://doi.org/10.3389/FRVIR.2021.611214

Wei Y, Zheng J, So RHY (2018) Allocating less attention to central vision during vection is correlated with less motion sickness. Ergonomics 61(7):933–946. https://doi.org/10.1080/00140139.2018.1427805

Wei Y, Okazaki YO, So RHY, Chu WCW, Kitajo K (2019) Motion sickness-susceptible participants exposed to coherent rotating dot patterns show excessive N2 amplitudes and impaired theta-band phase synchronization. Neuroimage 202:116028. https://doi.org/10.1016/j.neuroimage.2019.116028

Wei Y, Wang Y, Okazaki YO, Kitajo K, So RHY (2023) Motion sickness resistant people showed suppressed steady-state visually evoked potential (SSVEP) under vection-inducing stimulation. Cogn Neurodyn. https://doi.org/10.1007/s11571-023-09991-7

White DJ, Congedo M, Ciorciari J, Silberstein RB (2012) Brain oscillatory activity during spatial navigation: theta and gamma activity link medial temporal and parietal regions. J Cogn Neurosci 24:686–697. https://doi.org/10.1162/jocn_a_00098

Wilkins A (2016) A physiological basis for visual discomfort: application in lighting design. Light Res Technol 48(1):44–54. https://doi.org/10.1177/1477153515612526

Yeo SS, Park SY, Yun SH (2024) Investigating cortical activity during cybersickness by fnirs. Sci Rep 14(1):1–9. https://doi.org/10.1038/s41598-024-58715-2

Zhang WH, Chen A, Rasch MJ, Wu S (2016) Decentralized multisensory information integration in neural systems. J Neurosci 36(2):532–547. https://doi.org/10.1523/JNEUROSCI.0578-15.2016

Zhang WH, Wang H, Chen A, Gu Y, Lee TS, Wong KM, Wu S (2019) Complementary congruent and opposite neurons achieve concurrent multisensory integration and segregation. Elife. https://doi.org/10.7554/eLife.43753

Zhao Y (2017) *Identifying vestibular and visual cortical response during circular vection among people with different susceptibility to motion sickness* [The Hong Kong University of Science and Technology]. https://doi.org/10.14711/thesis-b1781036

Zhao Y, Wei Y, Wang Y, So RHY, Chan CCH, Cheung RTF, Wilkins A (2023) Identification of the human cerebral cortical hemodynamic response to passive whole-body movements using near-infrared spectroscopy. Front Neurol 14(December):1–11. https://doi.org/10.3389/fneur.2023.1280015